



1 The SP19 Chronology for the South Pole Ice Core - Part 1:
2 Volcanic matching and annual-layer counting

3

4 Dominic A. Winski^{1,2}, Tyler J. Fudge³, David G. Ferris⁴, Erich C. Osterberg⁴, John M.
5 Fegyveresi⁵, Jihong Cole-Dai⁶, Zayta Thundercloud⁴, Thomas S. Cox⁷, Karl J. Kreutz^{1,2},
6 Nikolas Ortman⁴, Christo Buizert⁸, Jenna Epifanio⁸, Edward J. Brook⁸, Ross Beaudette⁹,
7 Jeff Severinghaus⁹, Todd Sowers¹⁰, Eric J. Steig³, Emma C. Kahle³, Tyler R. Jones¹¹,
8 Valerie Morris¹¹, Murat Aydin¹², Melinda R. Nicewonger¹², Kimberly A. Casey^{13,14},
9 Richard B. Alley¹⁰, Edwin D. Waddington³, Nels A. Iverson¹⁵, Ryan C. Bay¹⁶, Joseph M.
10 Souney¹⁷

11 ¹*School of Earth and Climate Sciences, University of Maine, Orono, Maine, USA*

12 ²*Climate Change Institute, University of Maine, Orono, Maine, USA*

13 ³*Department of Earth and Space Sciences, University of Washington, Seattle,*
14 *Washington, USA*

15 ⁴*Department of Earth Sciences, Dartmouth College, Hanover, New Hampshire, USA*

16 ⁵*U.S. Army Corps of Engineers Cold Regions Research and Engineering Laboratory,*
17 *Hanover, New Hampshire, USA*

18 ⁶*Department of Chemistry and Biochemistry, South Dakota State University, Brookings,*
19 *South Dakota, USA*

20 ⁷*Physical Science Department, Butte College, Oroville, California, USA*

21 ⁸*College of Earth, Ocean and Atmospheric Sciences, Oregon State University, Corvallis,*
22 *Oregon, USA*

23 ⁹*Scripps Institution of Oceanography, UC San Diego, La Jolla, California, USA*

24 ¹⁰*Department of Geosciences and Earth and Environmental Systems Institute,*
25 *Pennsylvania State University, University Park, Pennsylvania, USA*

26 ¹¹*Institute of Arctic and Alpine Research, University of Colorado, Boulder, Colorado,*
27 *USA*

28 ¹²*Department of Earth System Science, UC Irvine, Irvine, California, USA*

29 ¹³*Earth Sciences Division, NASA Goddard Space Flight Center, Greenbelt, MD, USA*

30 ¹⁴**now at National Land Imaging Program, U.S. Geological Survey, Reston, VA, USA*

31 ¹⁵*New Mexico Institute of Mining and Technology, New Mexico Bureau of Geology and*
32 *Mineral Resources, Socorro, New Mexico, USA*

33 ¹⁶*Physics Department, University of California, Berkeley, California, USA*

34 ¹⁷*Institute for the Study of Earth, Oceans and Space, University of New Hampshire,*
35 *Durham, New Hampshire, USA*

36

37 Correspondence to: Dominic Winski (dominic.winski@maine.edu)

38



38 Abstract

39 The South Pole Ice Core (SPICEcore) was drilled in 2014-2016 to provide a
40 detailed multi-proxy archive of paleoclimate conditions in East Antarctica during the
41 Holocene and late Pleistocene. Interpretation of these records requires an accurate depth-
42 age relationship. Here, we present the SP19 timescale for the age of the ice of SPICEcore.
43 SP19 is synchronized to the WD2014 chronology from the West Antarctic Ice Sheet
44 Divide (WAIS Divide) ice core using stratigraphic matching of 251 volcanic events.
45 These events indicate an age of 54,302 +/- 519 years BP (before the year 1950) at the
46 bottom of SPICEcore. Annual layers identified in sodium and magnesium ions to 11,341
47 BP were used to interpolate between stratigraphic volcanic tie points, yielding an
48 annually-resolved chronology through the Holocene. Estimated timescale uncertainty
49 during the Holocene is less than 18 years relative to WD2014, with the exception of the
50 interval between 1800 to 3100 BP when uncertainty estimates reach +/- 25 years due to
51 widely spaced volcanic tie points. Prior to the Holocene, uncertainties remain within 124
52 years relative to WD2014. Results show an average Holocene accumulation rate of 7.4
53 cm/yr (water equivalent). The time variability of accumulation rate is consistent with
54 expectations for steady-state ice flow through the modern spatial pattern of accumulation
55 rate. Time variations in nitrate concentration, nitrate seasonal amplitude, and $\delta^{15}\text{N}$ of N_2
56 in turn are as expected for the accumulation-rate variations. The highly variable yet well-
57 constrained Holocene accumulation history at the site can help improve scientific
58 understanding of deposition-sensitive climate proxies such as $\delta^{15}\text{N}$ of N_2 and photolyzed
59 chemical compounds.

60 1. Introduction

61 Polar ice core records provide rich archives of paleoclimate information that have
62 been used to advance understanding of the climate system. One of the great strengths of
63 ice cores is the tightly constrained dating that permits interpretation of abrupt events and
64 comparisons of phasing among records. Therefore, a critical phase in the development of
65 any ice core record is the rigorous establishment of a depth-age relationship.

66 Several techniques are available to assign ages to each specific depth in an ice
67 core. These include annual layer identification of chemical (e.g. Sigl et al. 2016;
68 Andersen et al. 2006; Winstrup et al. 2012) and physical (e.g. Hogan and Gow 1997;
69 Alley et al. 1997) ice properties, identification of stratigraphic horizons as relative age
70 markers (e.g. Sigl et al. 2013; Bazin et al. 2013; Veres et al. 2013) and glaciological flow
71 modeling (e.g. Parrenin et al. 2004). To establish a depth-age relationship for the South
72 Pole Ice Core (hereafter SPICEcore), we use a combination of 1) annual layer counting of
73 glaciochemical tracers and 2) stratigraphic matching of volcanic horizons to the West
74 Antarctic Ice Sheet (WAIS) Divide ice core timescale “WD2014” (Sigl et al. 2016,
75 Buizert et al. 2015).

76 SPICEcore was drilled in 2014-2016 for the purpose of establishing proxy
77 reconstructions of temperature, accumulation, atmospheric circulation and composition,
78 and other earth system processes for the last 40,000 years (Casey et al. 2014). The
79 SPICEcore record is the only ice core south of 80° S extending into the Pleistocene and is
80 also located within one of the highest accumulation regions within interior East
81 Antarctica (Casey et al. 2014). This provides the unique opportunity to develop the most



82 highly resolved ice core record from interior East Antarctica. The South Pole is located at
83 an elevation of 2835 m (Casey et al. 2014) and has a mean annual temperature of -50°C
84 (Lazzara et al. 2012). The high accumulation rate at South Pole ($\sim 8 \text{ cm yr}^{-1}$ snow water
85 equivalent, Mosley-Thompson et al. 1999; Lilien et al. 2018) relative to most of interior
86 East Antarctica permits glaciochemical measurements at high temporal resolution.
87 Occasional cyclonic events, particularly during winter months, bring seasonally variable
88 amounts of sea salt, dust and other trace chemicals to the South Pole (Ferris et al. 2011;
89 Mosley-Thompson and Thompson 1982; Parungo et al. 1981; Hogan 1997). Due to the
90 favorable logistics and location at the geographic South Pole, the immediate area has
91 been the site of several previous ice coring campaigns (e.g. Korotkikh et al. 2014; Budner
92 and Cole-Dai 2003; Ferris et al. 2011; Meyerson et al. 2002; Mosley-Thompson and
93 Thompson 1982). These ice cores contain records spanning the last two millennia,
94 providing insight into seasonal chemistry variations and background values as well as
95 recent snow accumulation trends.

96 In this paper, we focus on dating the ice itself; the dating of the gas record and the
97 calculation of the gas-age/ice-age difference will be the subject of a future paper. The
98 procedures used to generate the data necessary for ice-core dating and the dating
99 techniques themselves are summarized in the remainder of the paper.

100

101 **2. Measurements and Ice core data**

102 *2.1 Measurements*

103 *2.1.1 Fieldwork and Preparation* Drilling began at the South Pole in the 2014/2015
104 austral summer season at a location 2.7 km from the Amundsen-Scott station, using the
105 Intermediate Depth Drill designed and deployed by the U.S. Ice Drilling Program
106 (Johnson et al. 2014). Drilling began at a depth of 5.10 m and reached a depth of 755 m
107 in January 2015. Drilling continued during the 2015/2016 season, reaching a final depth
108 of 1751 m. To extend the record to the surface, a 10 m core was hand-augered near the
109 location of the main borehole. Ice core sections with a diameter of 98 mm and length of
110 1 m were packaged and shipped to the National Science Foundation Ice Core Facility
111 (NSF-ICF) in Denver, Colorado. Each meter-long section of core was weighed and
112 measured to calculate density and assign core depth. The cores were cut using bandsaws
113 into CFA (continuous flow analysis) sticks with dimensions of 24 mm x 24 mm x 1 m
114 and packaged in clean room grade, ultra-low outgassing polyethylene layflat tubing
115 (Texas Technologies ULO) in preparation for the melter system at Dartmouth College.
116 An additional 13 mm x 13 mm x 1 m stick was used for water-isotope analyses at the
117 University of Colorado (see Jones et al., 2017 for water-isotope methods).

118

119 *2.1.2 ECM measurements* During core processing at the NSF-ICF, each core was cut and
120 planed horizontally to produce a smooth, flat surface (Souney et al., 2014). Electrical
121 conductivity measurements (ECM) were made with both direct current (DC) and
122 alternating current (AC). We report only AC-ECM here, as it was the primary
123 measurement for identifying volcanic peaks; further details are provided by Fudge et al.
124 (2016a). Multiple tracks were made at different horizontal positions across the core
125 (typically 3 tracks) and then averaged together. Measurements from each meter were



126 normalized by the median to preserve the volcanic signal while providing a consistent
127 baseline conductance to account for variations in electrode contact.

128

129 2.1.3 Visual Measurements Each core was examined by JF in a dark room with
130 illumination from below. For some cores, particularly for depths greater than ~250 m,
131 side-directed tray lighting using a scatter-diffuser was more effective at revealing
132 features. All noteworthy internal features, stratigraphy, physical properties and seasonal
133 indicators were documented by hand in paper log books.

134 Previous work at the South Pole shows that coarse-grained and/or depth-hoar
135 layers form annually in late summer, often capped by a bubble-free wind-crust or iced
136 crust up to ~1 mm thickness (Gow, 1965). We used these coarse-grained layers as the
137 annual “picks” (noted as late-summers). The stratigraphy in the core was generally
138 uniform and well-preserved, with the pattern identified by Gow (1965) continuing
139 downward. The depths of all noted features were recorded to the nearest millimeter. Full
140 details on visual layer counting are described in Fegyveresi et al. (2017).

141

142 2.1.4. Ice Core Chemistry Analyses Ice sticks were melted and samples collected at
143 Dartmouth College using a Continuous Flow Analysis – Discrete Sampling (CFA-DS)
144 melt system (Osterberg et al. 2006). Stick ends were decontaminated by scraping with
145 pre-cleaned ceramic (ZrO) knives. Cleaned sticks were then placed in pre-cleaned
146 holders and melted on a melt head regulated by a temperature controller in a standup
147 freezer. The melt head was made of 99.9995% pure chemical-vapor-deposited silicon
148 carbide (CVD-SIC). CVD-SIC was chosen because of its ultra-high purity, high thermal
149 conductivity, extreme hardness and excellent resistance to acids allowing for acid
150 cleaning when not in use. The melt head design includes a 16x16x3 mm high tiered and
151 rimmed inner section that was tapered with capillary slits to a center drain hole to
152 minimize the risks of contamination from outer meltwater and wicking when melting
153 porous firn (similar to Osterberg et al. 2006). This design provides a ≥4 mm buffer
154 between the exterior of each ice stick and the edge of the center tiered section. Flexible
155 plastic tines aligned on the four sides of the melt head keep the ice stick centered.

156 A peristaltic pump drew outer, contaminated meltwater away from the outer
157 section through four waste lines. A second peristaltic pump drew clean meltwater from
158 the center, tiered section of the melt head to a debubbler. The debubbler consisted of a
159 short section of porous expanded PTFE tubing (Zeus Aeos 0000143895) and utilized
160 pump pressure to force air through the tubing walls. The debubbled melt stream entered
161 a splitter where it was separated into three fractions: one for major ion analyses, another
162 for trace element analyses, and a third that passed through a particle counter and size
163 analyzer (Klotz Abakus), an electrical conductivity meter (Amber Science 3084), and a
164 flowmeter (Sensirion SLI-2000) before final collection in vials (Fig. 1). Samples were
165 collected in cleaned vials using Gilson FC204 fraction collectors (cleaning procedures
166 described in Osterberg et al. 2006). Samples were capped and kept frozen until
167 additional analysis.

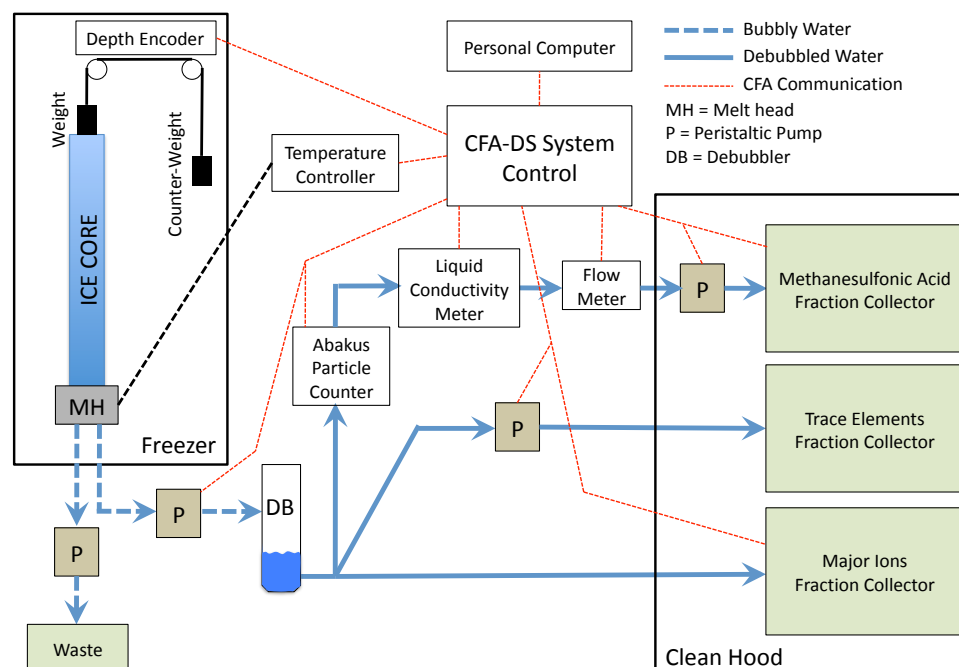
168 Core depths corresponding to each sample were tracked using custom software
169 expanding on the concept of depth-point tracking developed by Breton et al. (2012).
170 Simply, software tracks each depth point in the core as it progresses through the CFA-DS
171 system until it reaches each collection vial. This is accomplished by using a combination



172 of melt rate, flow rates, and system line volumes. Melt rates were measured with a
173 weighted rotary encoder tracking displacement as the ice stick melts. Flow rates were
174 measured by either an electronic flow meter or by calibrating the volume per revolution
175 of each peristaltic pump tubing. Fraction collector advancements were made
176 automatically based on melt rate, ice density (in firm), and the required sample volume
177 and frequency. In addition, the software collected data from the inline particle counter
178 and electronic conductivity meter. This system is capable of producing high-resolution,
179 ultra-clean samples and has been used successfully in previous studies (e.g. Osterberg et
180 al. 2017; Winski et al. 2017; Breton et al. 2012; Koffman et al. 2014). Samples
181 corresponding to the top and bottom of each stick were assigned depths equal to the top
182 and bottom depths measured at NSF-ICF, with intervening samples scaled linearly by the
183 ratio of the NSF-ICF core lengths over the lengths measured by the depth encoder. This
184 ensures that our data remain consistent with other SPICEcore datasets and there is no
185 possibility of drift due to scraping core breaks, measurement or encoder errors.

186 Discrete ion chemistry samples were collected every 1.1 cm on average for the
187 upper 800 m (Holocene) portion of the core and every 2.4 cm on average for older ice. In
188 total, 112,843 samples were collected and analyzed using a Thermo Fisher Dionex ICS-
189 5000 capillary ion chromatograph to determine the concentrations of the following major
190 ions: nitrate, sulfate, chloride, sodium, potassium, magnesium and calcium. Liquid
191 conductivity, particle concentration, and particle size distribution measurements were
192 taken continuously with an effective resolution of 3 mm.

193



194
195
196
197

Figure 1: A schematic representation of the Dartmouth ice core melter system.



198 **2.2 Chemistry Characteristics of SPICEcore**

199

200

201

202

203

204

205

206

207

208

209

210

211

212

213

214

215

216

217

218

219

220

221

222

223

224

225

226

227

228

229

230

231

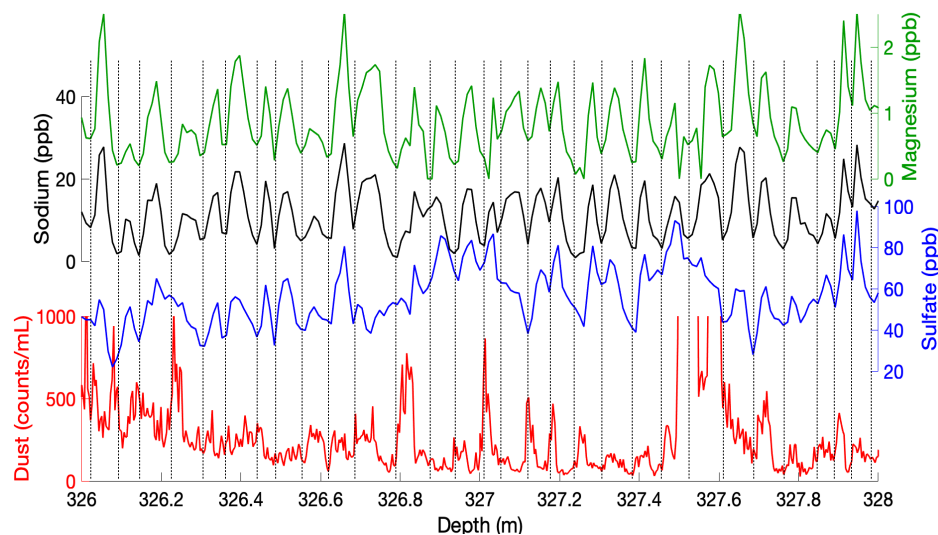
232

233

Previous research at the South Pole has shown that major sea salt ions (Cl^- , Na^+ , Mg^{2+}) have winter maxima and summer minima when compared with the position of summer depth hoar layers (Cole-Dai and Mosley-Thompson 1999; Ferris et al. 2011). The same conclusion was reached through comparisons with seasonal isotopic fluctuations: sodium and magnesium peaks coincide with seasonal water-isotope minima (Legrand and Delmas 1984; Whitlow et al. 1992). These observations are consistent with sea salt aerosol measurements collected at the South Pole that demonstrate large sodium influx during winter months (Bodhaine et al. 1986; Bergin et al. 1998). The same seasonal pattern of sea salt deposition has been observed in Holocene strata of the WAIS Divide ice core (Sigl et al. 2016) and in other Antarctic ice cores (Kreutz et al. 1997; Curran et al. 1998; Wagenbach et al. 1998; Udisti et al. 2012). In the uppermost firm, seasonal chemistry is also influenced by the operation of South Pole station and its associated logistics (Casey et al. 2017).

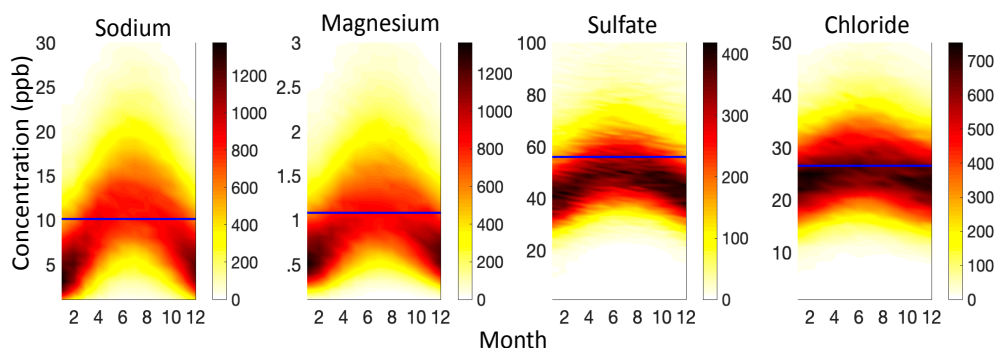
In SPICEcore, sampling resolution is sufficiently high to consistently detect annual cyclicity in glaciochemistry throughout the Holocene. Clear annual signals are present in several glaciochemical species to a depth of 798 m (approximately 11341 BP), with the most prominent in sodium and magnesium (Figs. 2-3), which covary ($r = 0.95$; $p < 0.01$) and have coherent annual maxima and minima. Sulfate, chloride, AC-ECM, liquid conductivity, particle count and visual stratigraphy all exhibit discernable annual cyclicity.

The South Pole has long been recognized as a favorable location for identifying volcanic events, reflected by previous work on South Pole paleovolcanism (Ferris et al. 2011; Delmas et al. 1992; Budner and Cole-Dai 2003; Cole-Dai et al. 2009; Baroni et al. 2008; Cole-Dai and Thompson 1999; Palais et al. 1990). Volcanic events in SPICEcore are evident as peaks in sulfate and ECM rising well above background values. Within the Holocene, the median annual sulfate maximum is 60 ppb. This background level increases deeper in the core to values as high as 131 ppb between 18-26 ka BP, despite the lack of annual resolution during the Pleistocene. In contrast, sulfate concentration in volcanic events regularly exceeds 200 ppb with occasional concentrations as high as 1000 ppb for very large signals. For example, the pair of eruptions in 135 and 141 BP (1815 and 1809 CE), attributed to Tambora and Unknown in previous Antarctic studies (Delmas et al. 1992; Cole-Dai et al. 2000; Sigl et al. 2013) have peak sulfate concentrations of 518 and 281 ppb respectively, emerging well above seasonal background values of 60 ppb.



234
235
236
237
238
239
240

Figure 2: Example of annual layering in a representative segment of SPICEcore. Depicted are magnesium (green) and sodium (black) concentrations showing nearly identical variations and clear annual cyclicality. Sulfate (blue) has consistent but less pronounced layering, and dust (red; 1 micron size bin) has occasionally visible annual layering. Vertical dashed lines show annual pick positions based on the data shown.



241
242
243
244
245
246
247
248
249
250
251
252

Figure 3: Seasonal variation in magnesium, sodium, sulfate and chloride ion concentration in SPICEcore from -42 to 11341 BP (11383 total years). In each panel, the horizontal axis is month of the year (with 0 being Jan. 1st) from linear interpolation between mean sample depth and the timescale. The vertical axis is concentration (ppb). The color scale indicates the density of measurements within gridded month and concentration bins. Concentration bin widths are 1 month (without claiming 1 month precision) and 1 ppb except for magnesium which is 0.1 ppb. The Holocene mean concentration of each ion is shown as a blue bar. Strong annual cyclicality is apparent in sodium and magnesium data. Annual cyclicality is weaker in sulfate and chloride data.

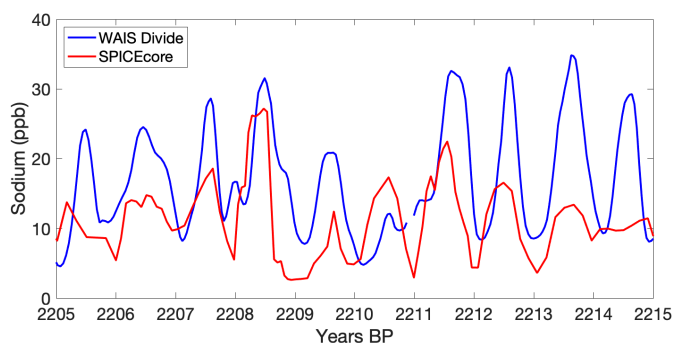


253 3. SPICEcore Dating Methods

254 3.1 Approach

255 The SPICEcore timescale (SP19) was developed by combining annual layer
256 counting with volcanic event matching between SPICEcore and the WAIS Divide
257 chronology. We identified 251 volcanic tie points that are clearly visible in both
258 SPICEcore and WAIS Divide (Sigl et al. 2016). These tie points link SP19 with the
259 WAIS Divide chronology, resulting in one of the most precisely dated interior East
260 Antarctic records. Above 798 m, ages are interpolated between volcanic tie points using
261 layer counts. Below 798 m, ages are interpolated between tie points by finding the
262 smoothest annual layer thickness profile (minimizing the second derivative) that satisfies
263 at least 95% of the tie points (following Fudge et al. 2014).

264 Although it is possible to create an independent, annually layer counted
265 SPICEcore timescale during the Holocene, we linked the entire SP19 chronology to the
266 WAIS Divide chronology for several reasons: (1) annual layers are insufficiently thick
267 below 798 m (approximately 11341 BP) to consistently resolve individual years,
268 requiring synchronization to another ice core to achieve the best possible dating accuracy.
269 Tying the entire SP19 chronology to the WAIS Divide core ensures consistent temporal
270 relationships between these two records; (2) although annual layers are remarkably well-
271 preserved in SPICEcore chemistry, WAIS Divide has a higher accumulation rate (Banta
272 et al., 2008; Fudge et al., 2016b; Koutnik et al. 2016) and stronger seasonality in
273 chemical constituents (Sigl et al. 2016), producing more robust annual layering (Figure
274 4); (3) it is expected that some years at South Pole experience very low accumulation,
275 resulting in a lack of an annually resolvable record during those years (Hamilton et al.
276 2004; Van der Veen et al. 1999; Mosley-Thompson et al. 1995, 1999); (4) an attempt to
277 independently date the Holocene annual layers created drift of several percent at
278 stratigraphic tie points. We therefore elected to anchor the SP19 timescale to WD2014,
279 and use the annual layer counts as a means of interpolating between WD2014 tie points
280 during the Holocene. The SP19 timescale spans -64 BP (2014 CE) to 54,302 +/- 519 BP,
281 with the annually-dated Holocene section of the core extending to 11341 BP (798 m
282 depth).



283

284 **Figure 4: Annual layering of sodium in WAIS Divide (blue) and SPICEcore (red). Annual**
285 **layers in sodium are clear in both records but are more pronounced at WAIS Divide for**
286 **most years.**



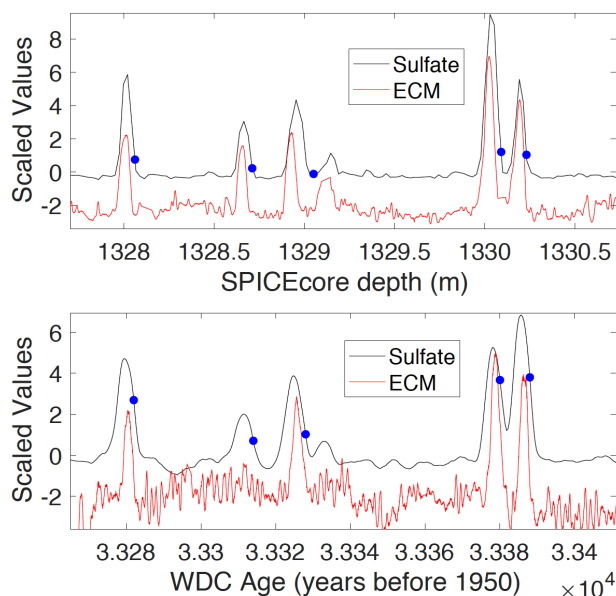
287 ***3.2 Procedure for identifying matching events***

288 The matching of volcanic events in sulfate and ECM records is commonly used to
289 synchronize ice core timescales (e.g. Severi et al., 2007, 2012; Fujita et al., 2015),
290 including the recent extension of the annually-resolved WAIS Divide timescale to East
291 Antarctic cores (Buizert et al., 2018). Volcanic matching is based on the depth pattern of
292 events more than the magnitude of the events because the magnitude in individual ice
293 cores can vary significantly across Antarctica depending on the location of the volcano
294 and atmospheric transport to the ice core site. The volcanic matching between SPICEcore
295 and WAIS Divide is based primarily on the sulfate record for SPICEcore and the
296 combined sulfur and sulfate records for WAIS Divide (Buizert et al. 2018). AC-ECM
297 from SPICEcore and WAIS Divide was used as a secondary data set and to fill small data
298 gaps in the sulfate record. An example of the four data sets is shown in Figure 5.
299 The volcanic matches were performed independently by two interpreters (TJF and DF)
300 and then reconciled by one (TJF) with concurrence from the other (DF). The position of
301 each match was defined as the inception of the sulfate rise in order to most consistently
302 reflect the timing of the volcanic event itself. Of the final 251 tie points, 229 were
303 identified in the sulfate data by both interpreters. Of the remaining matches, 14 were
304 made by one interpreter in the sulfate data, and at least one interpreter in the ECM data.
305 One of the other matches was made only with ECM because of a gap in the sulfate data
306 for SPICEcore. The last 7 matches were part of sequences not initially picked by one
307 interpreter but deemed to be sufficiently distinct from the other events in the sequence to
308 be included.

309 We note that the purpose of the volcanic matching was to develop a robust
310 SPICEcore timescale, not to assess volcanic forcing. Thus, there are many potential
311 volcanic matches that were not included either because they did not have the same level
312 of certainty as the final 251 matches, or because they were in close proximity to the final
313 matches and thus did not provide additional timescale constraints.

314 For the pre-Holocene section of the core, ages between the volcanic matches are
315 interpolated by finding the smoothest annual layer thickness by minimizing the second
316 derivative (Fudge et al., 2014). The goal of finding the smoothest annual layer thickness
317 time series is to prevent sharp changes affecting the apparent duration of climate events
318 on either side of a volcanic match point. The method allows the ages of the volcanic
319 matches to vary within a threshold to produce a smoother annual layer thickness
320 interpolation. The degree of smoothness was set such that 95% of the tie points are
321 shifted by 1-year or less, which is a reasonable uncertainty on the precision of the
322 volcanic matches.

323



324

325 **Figure 5: An example of volcanic matching between SPICEcore (top) and WAIS Divide**
326 **(bottom). Sulfate (black) and electrical conductivity (ECM; red) are shown for both ice**
327 **cores. Here, five events are shown that link specific depths in SPICEcore to known ages in**
328 **WAIS Divide. The position of the tie points is chosen at the beginning of the event (blue**
329 **circles). The y-axis values are scaled for ease of visualization and do not indicate absolute**
330 **measurement values.**

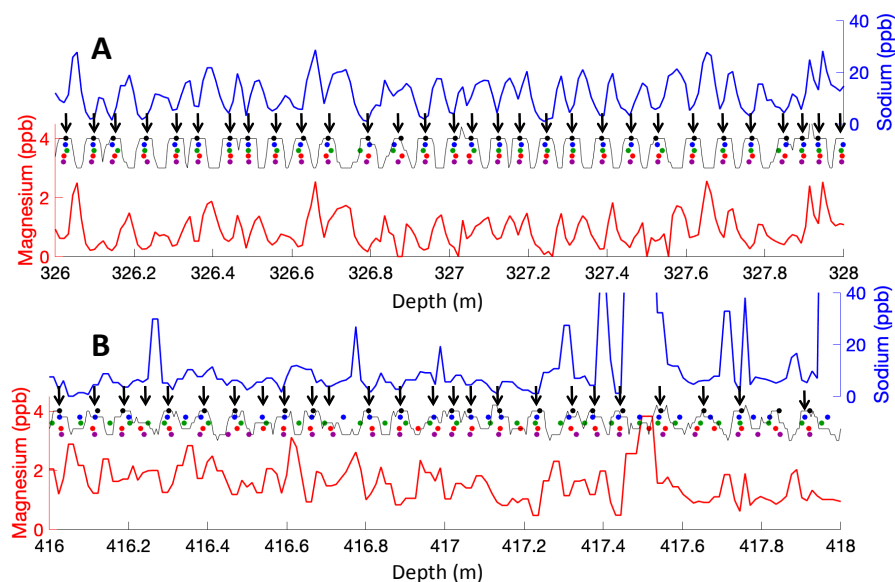
331 **3.3 Annual Layer Interpretation**

332 Annual layer counting in SPICEcore was initially done independently of the
333 volcanic matching with WAIS Divide. To minimize and quantify timescale uncertainty,
334 five interpreters performed the layer counting independently: DW, DF, TJJ, JF, and TC.
335 Sodium and magnesium were the primary annual indicators, but electrical conductivity,
336 dust concentration, sulfate, chloride and liquid conductivity were also helpful in
337 delineating individual years. To remain consistent, each interpreter agreed to place the
338 location of Jan. 1st for each year at the sodium/magnesium minimum, consistent with
339 previous interpretation of South Pole sea salt seasonality (e.g. Ferris et al. 2011; Bergin et
340 al. 1998). Two examples of annual layering including the Jan. 1st positions picked by
341 each interpreter are shown in Figure 6. Shown here are sections of high (A) and low (B)
342 agreement among the five interpreters.

343 This procedure resulted in five independent timescales to a depth of 540 m,
344 containing between 6529 and 6807 years. The details of reconciling the five independent
345 sets of layer counts are described in the Supplemental Information. Below 540 m, only
346 one author (DW) continued with the layer counting once the decision to use the annual
347 layers to interpolate between volcanic events had been made. The layer counting
348 procedure resulted in an annually resolved timescale, fully independent of any external
349 constraints, to a depth of 798.



350 Above 798 meters, 86 volcanic tie points were identified, producing 85 intervals
351 within which a known number of years must be present. To make the layer-counted
352 timescale consistent with these tie points, years were added or subtracted, as necessary,
353 within each interval such that the layer-counted timescale passed through each tie point
354 within ± 1 year of its age, linking SPICEcore with the WAIS divide chronology.
355 Procedural details for adding and subtracting layers by interval are discussed in the
356 Supplemental Information. In most intervals, few years needed to be added or subtracted,
357 with the average change in years equal to 5.6% of the interval length (Holocene intervals
358 ranged from 6 to 747 years). In certain sections layer counting consistently differed from
359 the WAIS-tied timescale. The most notable example is from 228 to 275 m depth where
360 105 years (14%) needed to be added.
361



362
363 **Figure 6: Representative sections of annual layer pick positions compared with magnesium**
364 **(red) and sodium (blue) concentrations. Each interpreter is represented with a different**
365 **color circle. Certain sections have excellent agreement among interpreters making**
366 **reconciliation trivial (A), whereas other sections have poorly defined annual signals and**
367 **associated disagreement among interpreters (B). The black line depicts the sum of all picks**
368 **within ± 2 cm; black arrows depict the final positions of the reconciled Jan. 1st annual**
369 **layer picks.**

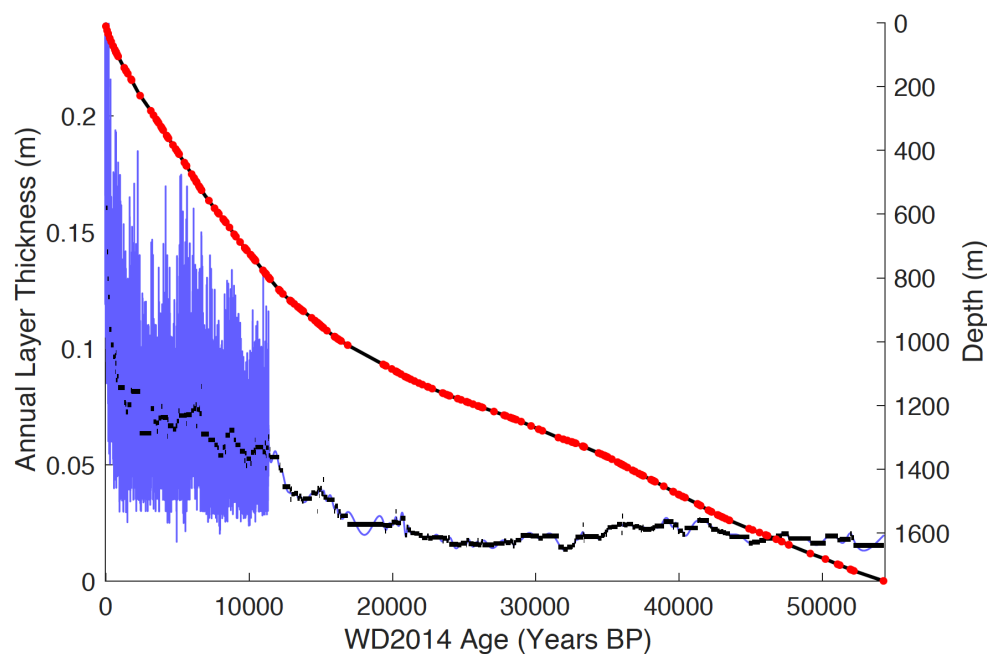
370 371 **4. Results and Discussion**

372 373 *4.1 Characteristics of the Timescale*

374
375 The SP19 chronology extends from 2014 CE (-64 BP) at the surface to 54302 BP
376 at 1751 m depth. The timescale and volcanic tie points are depicted in Figure 7 with
377 volcanic tie points pinning the timescale also shown. Annual layer thicknesses near the
378 surface are roughly 20 cm thick (owing to the low density of firn), decreasing rapidly to
379 ~ 8 cm/yr by the firn-ice transition. The timescale is annually resolved between -64 and



380 11341 BP, below which resolution varies based on the distance between tie points. Using
381 the methods in section 3.2 (Fudge et al. 2014), we report timescale values interpolated at
382 10-year resolution. The longest distance between tie points is 2476 years between 16348
383 and 19872 BP.



384 **Figure 7: The SP19 timescale, layer thickness and accumulation rate. The SP19 depth-age**
385 **relationship (right y-axis, black line) is constrained by volcanic events (red dots) extending**
386 **to 54302 BP. Annual layer thicknesses (left y-axis, blue) are shown at annual resolution**
387 **during the Holocene and as decadal-interpolated thicknesses based on the smoothest**
388 **annual layer thickness method (Fudge et al. 2014) during the Pleistocene. The average**
389 **annual layer thickness during each volcanic interval is shown in black for comparison.**
390
391

392 4.2 Uncertainties

393
394 In discussing uncertainty values for SP19, the reported values are uncertainty
395 *estimates* rather than rigorously quantified 1σ or 2σ values. There are several reasons for
396 this: 1) the chemicals used to count annual layers have similar cyclicity and are not
397 independent; 2) while each of the five interpreters counted layers independently, they
398 were likely employing similar strategies; 3) certain years may not be well-represented in
399 the data, providing insufficient information for accurate dating or quantifying
400 uncertainty; 4) volcanic events were identified in clusters such that each event is not
401 necessarily independent; 5) it is difficult to assign a numerical index of confidence to
402 specific volcanic tie points. Instead, we discuss timescale uncertainties as uncertainty
403 estimates, which are intended to approximate 2σ uncertainties but cannot be precisely
404 defined as such. This approach follows that of Sigl et al. (2016).

405 We assess the SP19 timescale uncertainty with respect to the previously published
406 WD2014 timescale (Sigl et al. 2016; Buizert et al. 2015). The absolute age uncertainty



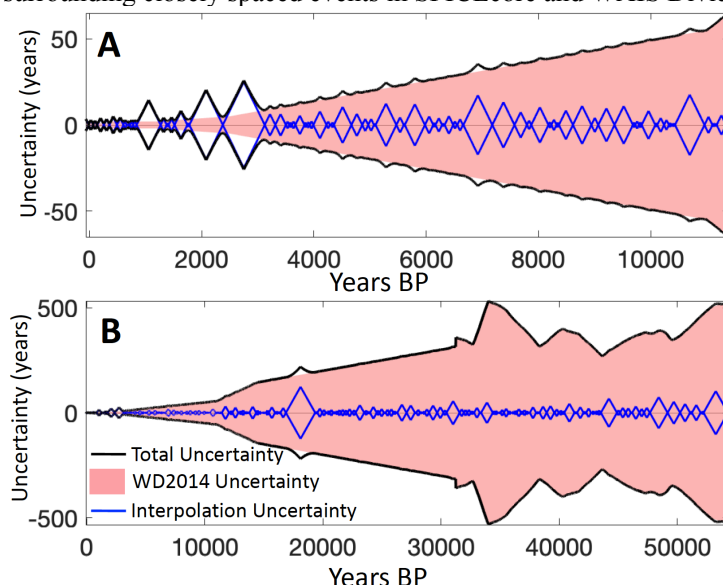
407 will always be equal to or greater than the uncertainty already associated with WD2014
408 (Buizert et al. 2015; Sigl et al. 2016; Fig. 8). In addition to the uncertainty in WD2014,
409 there is also uncertainty in our ability to interpolate between stratigraphic tie points.
410 During the Holocene, our layer-counting of sodium and magnesium concentration
411 improves the timescale accuracy between tie points. Interpolation uncertainty can be
412 estimated using the drift among the five different interpreters. We calculate the number
413 of years picked by each interpreter in running intervals of 500 years in the final WD2014
414 synchronized timescale. Under ideal conditions, each interpreter would also pick 500
415 years within each interval, but on average the number of years picked by interpreters
416 differs from the final timescale by 6.7%, usually by undercounting. This is similar to the
417 metric described in section 3.3, wherein the average change in years needed to reconcile
418 the layer counts and volcanic tie points was 5.6% of the interval length. Here, we report
419 the larger and more conservative value of 6.7%. If our layer counting skill drifts by +/-
420 6.7% while unconstrained by volcanic tie points, then the interpolation uncertainties
421 remain within +/- 18 years of WAIS Divide throughout the Holocene with the exception
422 of a poorly-constrained interval between approximately 1800-3100 BP. The maximum
423 uncertainty within the Holocene is +/- 25 years, occurring at roughly 2750 BP, where the
424 nearest tie points are 373 years away at 2376 and 3123 BP. This relationship can be
425 applied across the Holocene, with layers accumulating an uncertainty value equal to 6.7%
426 of the distance to the nearest tie point (Fig. 8; blue).

427 Below the Holocene (798 m depth), there were no annual layers to aid in our
428 interpolation of the timescale, leading to larger uncertainties. Our assumption of the
429 smoothest annual layer thickness (Fudge et al. 2014) satisfying tie points is the most
430 accurate interpolation method in the absence of additional information, at least in
431 Antarctic ice (Fudge et al. 2014). Using the WAIS Divide ice core as a test case, Fudge
432 et al. (2014) estimated that the interpolation method accumulates uncertainties at a rate of
433 10% of the distance to the nearest tie-point, roughly 50% faster than the uncertainty of
434 periods with identifiable annual layers. The longest interval with no volcanic constraints
435 is between 16348 and 19872 BP. At 18110 BP, the center of the interval, the
436 interpolation uncertainty reaches a maximum of 124 years, although uncertainties are
437 proportionally lower in other intervals with closer volcanic tie points.

438 Figure 8 shows the total uncertainty estimates associated with the SP19
439 chronology, with interpolation uncertainties added to the published WAIS Divide
440 uncertainties. The WD2014 and interpolation uncertainties are added in quadrature since
441 the two sources of uncertainty are independent. The maximum estimated uncertainty in
442 SP19 is 533 years at 34050 BP, the majority of which is attributed to uncertainties in
443 WD2014. While it is not possible to rigorously quantify uncertainties throughout SP19,
444 we believe these estimates provide reasonable and conservative values suitable for most
445 paleoclimate applications. We acknowledge there is additional uncertainty related to the
446 accuracy of our assigned stratigraphic tie points. Because of the conservative procedures
447 discussed in section 3.1 wherein only unambiguous matches were used in linking the
448 WAIS Divide and SPICEcore timescales, it is unlikely that any of these matches are in
449 error. In previous work (Ruth et al. 2007), potential errors associated with tie points have
450 been estimated by removing each tie point one at a time, and interpolating between the
451 new series of tie points (with one point missing). If this procedure is repeated for each tie
452 point and for each depth, the maximum error in age resulting from the erroneous



453 inclusion of a tie point is approximately 83 years. However, because clusters of volcanic
454 events were used to match the WAIS Divide and SPICEcore records, each tie point is not
455 necessarily independent. Therefore, this method is more useful at sections of widely
456 spaced tie points with greater potential uncertainties, but underestimates the uncertainties
457 surrounding closely spaced events in SPICEcore and WAIS Divide.



458
459 **Figure 8: Uncertainty estimates in the SP19 timescale. The pink shading indicates the**
460 **published uncertainty associated with the WAIS Divide timescale. The blue lines indicate**
461 **the estimated uncertainty due to interpolation by layer counting (Holocene) and by finding**
462 **the smoothest annual layer thickness history (Fudge et al. 2014; Pleistocene). Total**
463 **uncertainty (black) is defined here as the root sum of the squares of the interpolation and**
464 **WD2014 uncertainties. Total uncertainty estimates remain within +/- 50 years for most of**
465 **the Holocene (A), but are as high as 533 years in the Pleistocene (B).**

466 467 *4.3 Comparison with Visual Stratigraphy*

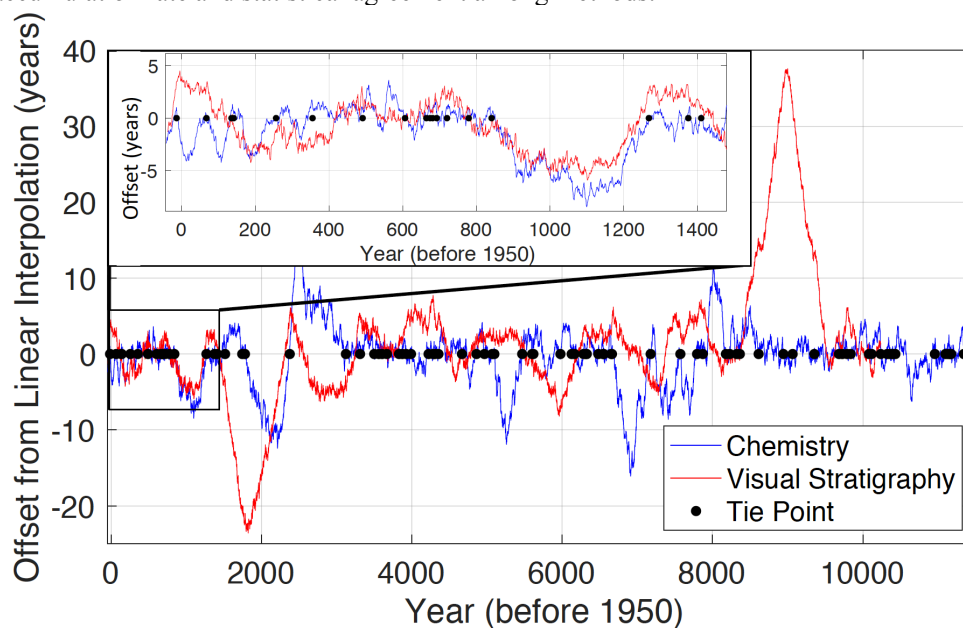
468
469 Visual stratigraphy in SPICEcore provides an independent check on the
470 glaciochemical layer counting we used to interpolate the Holocene depth-age scale
471 between tie points. Visual layer counting was conducted to a depth of 735 m (~10,250
472 years BP; Fegyveresi et al. 2017). We calculate the offset between the visual stratigraphic
473 timescale and a linear interpolation between tie points and do the same for the chemistry
474 layer counts (Fig. 9). If both the chemical and visual layer counting methods are
475 capturing the true variability in layer thickness within intervals, then both would show the
476 same structure within each interval.

477 There is broad correspondence between visual and chemical stratigraphy at all
478 depths, which, with their almost completely independent origin and measurements
479 techniques, is highly reassuring. In detail, though, there is little high-frequency
480 correspondence between visual and chemical layer counts below 1400 BP (150 m depth),
481 although a direct comparison is not possible since visible layer counts were not linked to



482 stratigraphic tie points between 1400-2400 BP and 8400-9500 BP. Furthermore, visible
483 layer counts were matched to the tie points within error of the WAIS Divide timescale,
484 whereas the chemistry layer counts were forced to match within +/- 1 year of each tie
485 point. In counting visible layers, occasional under- and overcounting of depth hoar layers
486 within annual strata is likely, especially in deeper ice where thinning will make adjacent
487 layers appear even closer. There were some intervals (e.g. 2000 – 2500 BP) in the core
488 that appeared more homogeneous during viewing, and therefore annual layer choices
489 have a higher level of uncertainty. Because of the differences between methodologies in
490 matching to tie points and because of the uncertainties in visual counting below 2000 BP
491 (200 m), we did not attempt to reconcile the visible and chemical layer counts, but
492 instead rely only on the annual layers in the chemistry data.

493 Between 100 and 1400 BP, both visible and glaciochemical timescales remain
494 remarkably coherent and do not indicate drift of more than +/- 2 years. Over this interval,
495 the correlation between the visible and chemical layer offsets from constant annual layer
496 thickness (red and blue curves in Figure 9) is 0.74. The correlation between the two layer
497 counting methods is as high as $r = 0.85$ between the tie points at 841 and 1268 BP. The
498 discrepancy within the top 100 years is due to the tie point at 10.58 m, which was not
499 included at the time of visible layer counting, as well as low layer chemical counting
500 confidence within the firn column. There is no obvious relation between the
501 accumulation rate and statistical agreement among methods.



502
503 **Figure 9: Comparison between visible layer (red) and chemistry-based (blue) Holocene**
504 **annual timescales. Both curves are shown as residual values with respect to a linear**
505 **interpolation between tie points (black circles). When the shape of the red and blue curves**
506 **is similar between tie points, we infer relatively high accuracy in both methods. The region**
507 **showing the closest agreement between methods is shown in the inset with both curves**
508 **remaining within 2 years of each other despite a long section with no tie points (841 to 1286**
509 **BP).**



510 **4.4 Accumulation Rate History**

511

512

513

514

515

516

517

518

519

520

521

522

523

524

525

526

527

528

529

530

531

532

533

534

535

536

537

538

539

540

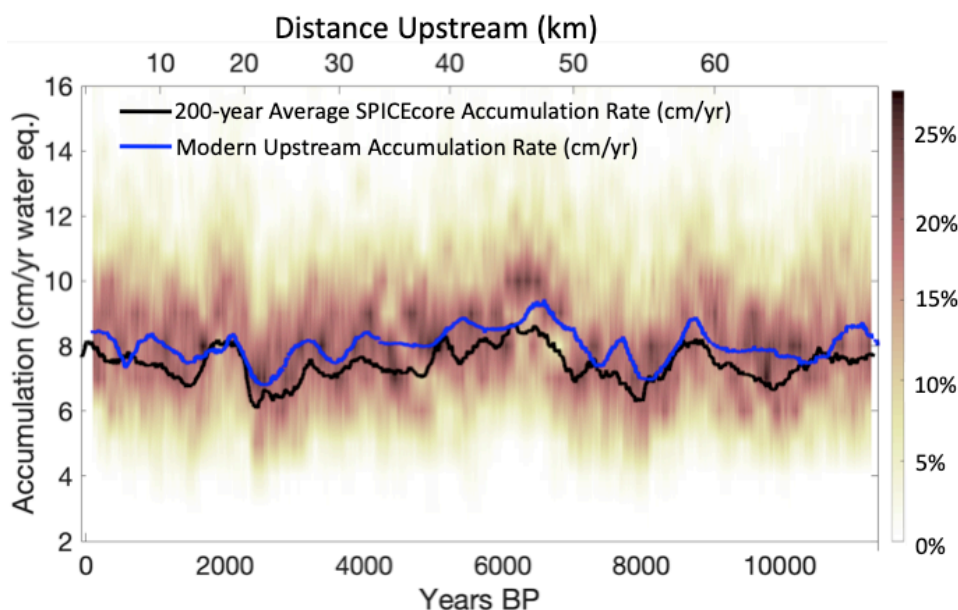
541

542

543

The SP19 timescale allows us to produce annually-resolved estimates of past snow accumulation to 11341 BP (Fig. 10). We apply a Dansgaard-Johnsen model (Dansgaard et al. 1969) to estimate the amount of thinning undergone by each layer of ice. Since the entirety of the Holocene in SPICEcore is located within the top third of the core (over 1900 m above the bed), the challenges associated with reconstructing surface accumulation are smaller than at sites with records closer to the bed (e.g. Kaspari et al. 2008, Thompson et al. 1998, Winski et al. 2017). Radar measurements indicate a bed depth at the South Pole of 2812 m, giving an ice-equivalent thickness of 2774 m, using the South Pole density function developed by Kuivinen et al. (1982). We used a kink height of 20% of the ice thickness and an input surface accumulation rate of 8 cm/yr, consistent with the parameters used by Lilien et al. (2018). The average Holocene accumulation rate is 7.4 cm/yr, in excellent agreement with results of previous studies (Hogan and Gow 1997; 7.5 cm/yr to 2000 BP; Mosley-Thompson et al. 1999 – 6.5-8.5 cm/yr for late 20th century). The upstream flow dynamics are too complicated for a static 1-D model to accurately determine the thinning function before the Holocene.

As discussed in Lilien et al. (2018), Koutnik et al. (2016), and Waddington et al. (2007), South Pole layer thicknesses are affected by 1) spatial variability in surface accumulation being advected to South Pole; 2) past climate-related changes in snow accumulation; and 3) post-depositional thinning due to ice flow. Thinning models can account for only the third factor. Understanding of Holocene climate history as recorded at other sites and in other indicators in SPICEcore, combined with knowledge of the modern upglacier variation in accumulation (Lilien et al., 2018), make it clear that the Holocene SPICEcore time-variations in accumulation are primarily from advection of spatial variations. Figure 10 shows Holocene accumulation rate in SPICEcore (black) compared with geophysically derived accumulation estimates over space using ice-penetrating radar (blue, details in Lilien et al. 2018). Using the present-day surface velocity field and the inferred 15% increase in flow rate, present day upstream surface accumulation rates were matched with corresponding ages at the SPICEcore borehole (Lilien et al. 2018). The close match between present-day near-surface accumulation rates upstream and the annual accumulation rate in SPICEcore shows that the millennial-scale signal of accumulation rate in SPICEcore is related to spatial patterns of snow accumulation upstream of South Pole.



544
545 **Figure 10: The Holocene accumulation rate history in SPICEcore. Shading indicates a**
546 **running histogram of accumulation rate with darker colors indicative of more years at a**
547 **given accumulation rate. The color axis (left) indicates percentage of years with a given**
548 **accumulation rate within 1 cm accumulation bins across 200-year sliding intervals. The**
549 **solid black line is the 200-year running mean of accumulation rate. These data are**
550 **compared with modern spatial accumulation rates upstream of SPICEcore (blue; upper x-**
551 **axis; Lilien et al. 2018).**

552 A striking feature in the Holocene accumulation record in SPICEcore is the sharp
553 dip centered on 2400 BP. Annual layers were notably less clear in that portion of
554 SPICEcore because low accumulation rates led to low sampling resolution (5-6
555 samples/year). For instance, in the interval between 228-275 m, the interpreters picked
556 between 511 and 670 years, when 747 years are present based on the volcanic tie points.
557 The cause of the sharp drop in accumulation is not clear. Modern accumulation rates
558 upstream of SPICEcore were measured using a 20 m-deep isochron imaged with ice
559 penetrating radar (Lilien et al. 2018). These results show lower accumulation in the
560 location where the 2400 BP ice originated (Fig. 10). However, the modern upstream
561 spatial pattern of accumulation shows a decline that is both more gradual and less than
562 half the magnitude of the 2400 BP change in SPICEcore. It is possible that this represents
563 a climatic signal, but we note sharp accumulation variations at this time that are not
564 observed in the WAIS Divide core (Fudge et al. 2016b; Koutnik et al. 2016). Instead, we
565 hypothesize that this event was most likely a transient local accumulation anomaly.
566 Farther upstream at ~75km from South Pole, there is an accumulation low where the rate of
567 change is approximately 3 cm/yr in 2 km. With the current South Pole ice flow
568 velocity of 10 m/yr, this could explain a 3 cm/yr decrease in 200 years, similar to what is
569 observed at 2400 BP. If a climate-driven accumulation anomaly did contribute to this
570 sharp change, these anomalies do not appear to be common, as we see no other large and
571 sustained change in the annual timescale.



572 On sub-centennial timescales, the effects of upstream advection of spatial
573 accumulation patterns are likely smaller, such that annual-to-decadal patterns in snow
574 accumulation in SPICEcore may be indicative of climate conditions. Previous studies
575 have used a snow stake field 400 m to the east (upwind) of South Pole station to assess
576 recent trends in accumulation rate with differing results. Mosley-Thompson et al. (1995,
577 1999) found a trend of increasing snow accumulation during the late 20th century, while
578 Monaghan et al. (2006) and Lazzara et al. (2012) found decreasing snow accumulation
579 trends between 1985-2005 and 1983-2010, respectively. No significant trends exist in the
580 SPICEcore accumulation record within the last 50 years, although there is a significant (p
581 = 0.046) increasing trend in snow accumulation in SPICEcore since 1900. Note that
582 errors in measured firn density would influence this accumulation trend.

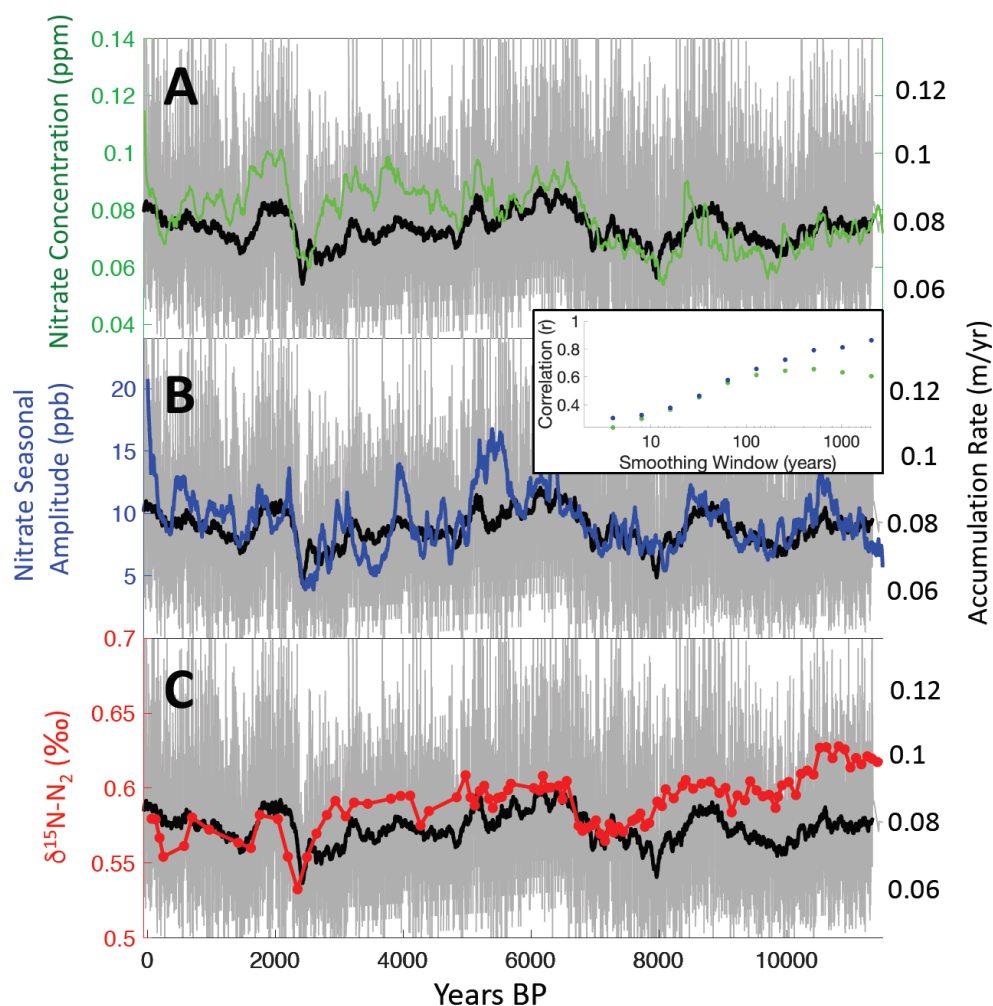
583

584 *4.5 Nitrate Variability, $\delta^{15}\text{N}$ of N_2 , and Accumulation*

585

586 SPICEcore nitrate concentrations provide independent support for the Holocene
587 accumulation rate history implied by the SP19 timescale. Previous studies have
588 recognized an association between accumulation rate and nitrate concentration among ice
589 core sites (Rothlisberger et al. 2002). Nitrate in surface snow, exposed to sunlight, results
590 in photolytic reactions that volatilize nitrate and release it to the atmosphere (Erbland et
591 al. 2013, Grannas et al. 2007; Rothlisberger et al. 2000). Evaporation of HNO_3 may also
592 significantly contribute to nitrate loss in the surface snow (Munger et al. 1999; Grannas et
593 al. 2007). Under low-accumulation conditions such as in East Antarctica, the amount of
594 time snow is exposed at the surface is the dominant control on nitrate concentration, such
595 that with more accumulation, snow is more rapidly buried and retains higher nitrate
596 concentrations (Rothlisberger et al. 2000).

597 There is close correspondence between accumulation rate and nitrate
598 concentration in SPICEcore (Fig. 11A). This association is strongest on multidecadal to
599 multicentennial timescales with correlation coefficients between accumulation rate and
600 nitrate reaching peak values after 512-year smoothing ($r = 0.60$; Fig. 11 inset). Although
601 the smoothing makes standard metrics statistical significance inapplicable, the similarity
602 between time series is expected given the previous work described above. Among sites,
603 an inverse relationship exists between seasonal amplitude of nitrate concentration and
604 accumulation rate. High-accumulation sites such as Summit, Greenland exhibit strong
605 annual nitrate layering, whereas low-accumulation sites such as Vostok (~ 2 cm w.e./yr;
606 Ekaykin et al. 2004) and Dome C (~ 3.6 cm w.e./yr; Petit et al. 1982) do not show annual
607 nitrate layers at all (Rothlisberger et al. 2000). SPICEcore has much higher accumulation
608 rates than Vostok or Dome C, and retains weak seasonality in nitrate wherein nitrate
609 often peaks in the summer months, the mechanisms for which are complex (Grannas et
610 al. 2007; Davis et al. 2004). As expected, the seasonal amplitude of nitrate over the
611 Holocene closely follows nitrate concentration and accumulation rate (Figure 11B) and is
612 even more highly correlated with accumulation than nitrate concentration itself,
613 especially on multicentennial to millennial timescales ($r = 0.80$ at 512-year smoothing).
614 Nitrate and accumulation rate are entirely independent variables in terms of their
615 measurement, adding confidence to the annual layer counting and tie points underlying
616 the SP19 chronology.

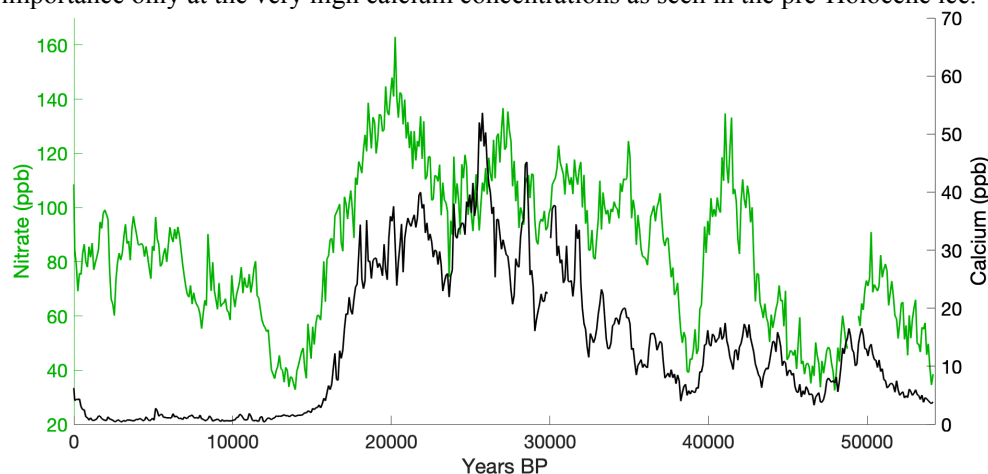


617
618 **Figure 11: The Holocene accumulation rate at the South Pole compared with nitrate and**
619 **$\delta^{15}\text{N}$.** In each panel, annual accumulation rates are depicted in gray, with the running 100-
620 year mean shown in black. These results are compared with 100-year median annual values
621 of nitrate concentration (A) and seasonal amplitude in nitrate concentration (B) as well as
622 $\delta^{15}\text{N}$ values (C). All three metrics exhibit shared variability on multicentennial to millennial
623 timescales. The inset shows the correlation between accumulation rate and nitrate
624 concentration (green) from panel A, and between accumulation rate and nitrate seasonal
625 amplitude (blue) from panel B, against length of the smoothing window, with both
626 exhibiting high correlations, especially at lower frequencies.
627

628 The relationship between inferred variations in accumulation rate and nitrate
629 concentration breaks down prior to the Holocene, but a relationship between nitrate and
630 calcium concentrations emerges. During the Pleistocene, the correlation between
631 centennial median of calcium and nitrate is $r = 0.80$ ($p < 0.01$; Figure 12), compared with
632 $r = 0.26$ ($p < 0.01$) during the Holocene. Rothlisberger et al. (2000, 2002) observed the



633 same pattern at Dome C, and attributed it to the stabilization of nitrate through interaction
634 with calcium and dust. They proposed that CaCO_3 and HNO_3 react to form $\text{Ca}(\text{NO}_3)_2$,
635 which is more resistant to photolysis and consequently leads to higher concentrations of
636 nitrate in the glacial age snowpack despite lower accumulation rates. The stabilization
637 effect of calcium apparently overtakes photolysis and evaporation of nitrate in terms of
638 importance only at the very high calcium concentrations as seen in the pre-Holocene ice.



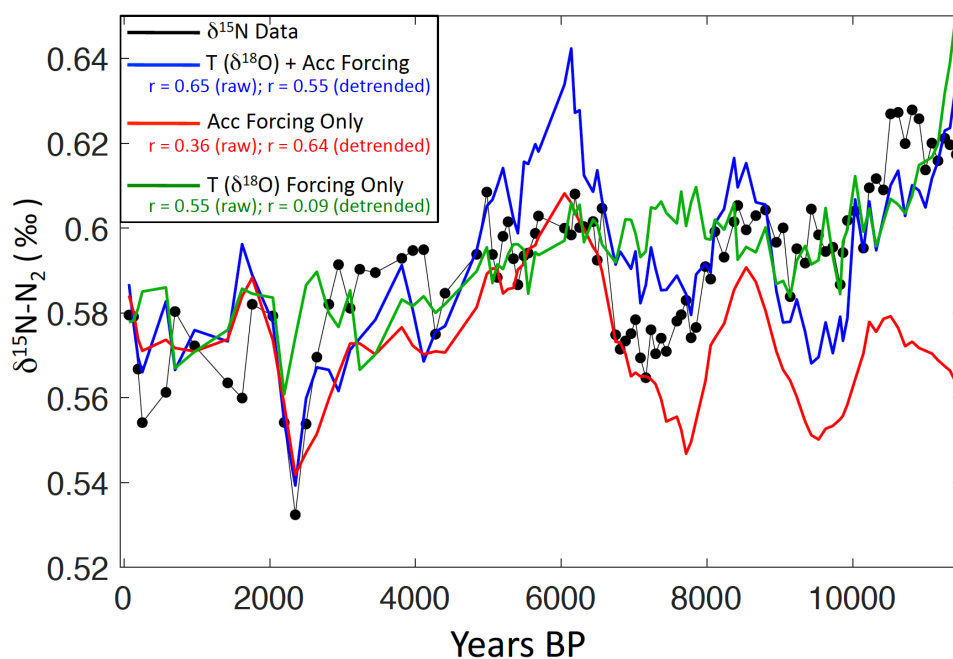
639 **Figure 12: Nitrate and calcium concentrations in SPICEcore. There is low centennial-scale**
640 **correlation ($r = 0.26$; $p < 0.01$) between calcium and nitrate ions during the Holocene, when**
641 **accumulation is the dominant control on nitrate concentration (Fig. 11). During the**
642 **Pleistocene, centennial median nitrate and calcium are positively correlated ($r = 0.80$; $p <$**
643 **0.01).**
644

645
646 Stable isotope ratios of atmospheric diatomic nitrogen ($\delta^{15}\text{N-N}_2$) in trapped air in
647 SPICEcore show a pattern similar to accumulation rate within the Holocene (Fig. 11C).
648 $\delta^{15}\text{N-N}_2$ values were measured using the procedures described by Petrenko et al. (2006).
649 The $\delta^{15}\text{N-N}_2$ in ice cores is driven by gravitational enrichment and is a proxy for past
650 thickness of the firm column (Sowers et al 1992). Firm densification rates depend
651 primarily on temperature and overburden pressure, with the second parameter closely
652 linked to the accumulation rate at the site. Low temperatures and high accumulation rates
653 both act to thicken the firm, thereby increasing $\delta^{15}\text{N-N}_2$ (Herron and Langway 1980,
654 Goujon 2003).

655 We perform a simple attribution study to see whether $\delta^{15}\text{N-N}_2$ variations can be
656 explained by reconstructed accumulation history or variable temperature. We compare
657 three climatic scenarios in a dynamical version of the Herron-Langway densification
658 model (Buizert et al. 2014). The first uses variable temperature (from $\delta^{18}\text{O}$ using a
659 scaling ratio of $0.8\text{‰}/^\circ\text{C}$) and variable accumulation (from annual layer thickness)
660 forcing; a second uses constant temperature (-51.5°C) and the variable accumulation
661 forcing; a third uses variable temperature and constant accumulation (7.8 cm/yr) forcing.
662 The correlations between the $\delta^{15}\text{N-N}_2$ data and each model run are displayed in Fig. 13
663 for both raw and detrended time series. The model scenario forced by both temperature
664 and accumulation has the best correspondence with the $\delta^{15}\text{N-N}_2$ data ($r = 0.65$; $p < 0.01$).
665 While secular changes in temperature appear to be driving the decreasing trend in $\delta^{15}\text{N-N}_2$



666 N_2 , millennial-scale fluctuations in $\delta^{15}N-N_2$ appear to be driven by accumulation,
667 supported by the high correlation ($r = 0.64$; $p < 0.01$) with the accumulation-only model
668 run using detrended time series. In particular, a sharp drop in $\delta^{15}N-N_2$ is present at
669 approximately 2400 BP, coincident with (and driven by) the local minimum in
670 accumulation. These experiments provide additional confidence in the reconstructed
671 accumulation history. To our knowledge, these data represent the best observation of
672 accumulation-driven $\delta^{15}N-N_2$ variation, making it a valuable target for benchmarking firm
673 densification model performance (Lundin et al. 2017).



674
675 **Figure 13: Results from three firm models compared with $\delta^{15}N$ variations in SPICEcore**
676 **(black). The model run incorporating only $\delta^{18}O$ -based temperature (green) does not**
677 **capture the millennial-scale variations in $\delta^{15}N$, whereas the models using only accumulation**
678 **(red) and both accumulation and $\delta^{18}O$ -based temperature (blue) are able to reproduce the**
679 **observed millennial-scale $\delta^{15}N$ changes. Correlations between the $\delta^{15}N$ data and the three**
680 **model runs are reported in the legend with correlation coefficients calculated for both raw**
681 **and linearly detrended time series.**
682

683 5. Summary

684 The SP19 includes the last 54,366 (-64 to 54,302 BP) years, and is the oldest and
685 most well-constrained ice core timescale from the South Pole. SP19 was developed using
686 251 volcanic events that link the SPICEcore timescale with the WAIS Divide chronology
687 WD2014 (Sigl et al. 2016; Buizert et al. 2015). High-resolution chemical records in
688 SPICEcore during the Holocene provide the only annually resolved full-Holocene
689 paleoclimate record in interior East Antarctica. Within the Holocene, SP19 uncertainties



690 are in the range of +/- 18 years with respect to WAIS Divide, with the exception of the
691 interval between 1800-3100 BP when low accumulation and sparse volcanic controls lead
692 to uncertainties as high as +/- 25 years. During the Pleistocene, SP19 uncertainties are
693 inversely related to the density of tie points, with maximum uncertainties reaching +/-
694 124 years relative to WD2014. Results show an average Holocene accumulation rate of
695 7.4 cm/yr with millennial-scale variations that are closely linked with advection of spatial
696 surface-accumulation patterns upstream of the drill site. Nitrate concentrations, nitrate
697 seasonal amplitude, and $\delta^{15}\text{N-N}_2$ variability are positively correlated with accumulation
698 rate during the Holocene, providing independent confirmation of the SP19 chronology.

699 **Competing Interests**

700 The authors declare that they have no conflict of interest.

701 **Data Availability**

702 The SP19 chronology, associated tie points, uncertainty estimates and supporting data
703 sets will be archived at the National Climate Data Center (www.ncdc.noaa.gov) and the
704 U.S. Antarctic Program Data Center (<http://www.usap-dc.org>) with the publication of this
705 paper.

706 **Author Roles**

707 All authors contributed data to this study. DW, DF, EO, JCD, ZT, KK, and NO
708 measured the ice core chemistry. TJF and EDW collected the ECM data. JF and RA
709 performed the visual analysis. CB, JE, EB, RB, JF and TS made the gas measurements.
710 ES, EK, TJ, and VM made the isotope measurements. DW, TJF, DF, JF and TC
711 performed the annual layer counting. TJF and DF performed the volcanic matching.
712 DW, TJF, DF, EO, JF and CB wrote the paper with contributions from all authors.

713 **Acknowledgements**

714 This work was funded through U.S. National Science Foundation grants 1443105,
715 1141839 (Steig), 1443336 (Osterberg), 1443397 (Kreutz), 1443663 (Cole-Dai), 1443232
716 (Waddington, Fudge), 1142517, 1443470 (Aydin), 1443464 (Sowers), 1443710
717 (Severinghaus), 1542778 (Alley, Fegyveresi), 1443472, 1643722 (Brook). We thank
718 Mark Twickler and the SPICEcore Science Coordination Office for administering the
719 project; the U.S. Ice Drill Program Office for recovering the ice core; the 109th New
720 York Air National Guard for airlift in Antarctica; the field team who helped collect the
721 core; the members of South Pole station who facilitated the field operations; National
722 Science Foundation Ice Core Facility for ice core processing; and the many student
723 researchers who produced the data underlying the SP19 timescale.

724
725
726
727
728
729



730 **References**

- 731 Alley, R. B., Shuman, C. A., Meese, D. A., Gow, A. J., Taylor, K. C., Cuffey, K. M., Fitzpatrick,
732 J. J., Grootes, P. M., Zielinski, G. A., and Ram, M.: Visual-stratigraphic dating of the GISP2 ice
733 core: Basis, reproducibility, and application, *Journal of Geophysical Research: Oceans*, 102,
734 26367-26381, 1997.
- 735 Andersen, K. K., Svensson, A., Johnsen, S. J., Rasmussen, S. O., Bigler, M., Röthlisberger, R.,
736 Ruth, U., Siggaard-Andersen, M.-L., Steffensen, J. P., and Dahl-Jensen, D.: The Greenland ice
737 core chronology 2005, 15–42 ka. Part 1: constructing the time scale, *Quat. Sci. Rev.*, 25, 3246-
738 3257, 2006.
- 739 Banta, J. R., McConnell, J. R., Frey, M. M., Bales, R. C., and Taylor, K.: Spatial and temporal
740 variability in snow accumulation at the West Antarctic Ice Sheet Divide over recent centuries,
741 *Journal of Geophysical Research: Atmospheres*, 113, 2008.
- 742 Baroni, M., Savarino, J., Cole-Dai, J., Rai, V. K., and Thiemens, M. H.: Anomalous sulfur
743 isotope compositions of volcanic sulfate over the last millennium in Antarctic ice cores, *Journal*
744 *of Geophysical Research: Atmospheres*, 113, 2008.
- 745 Bazin, L., Landais, A., Lemieux-Dudon, B., Kele, H. T. M., Veres, D., Parrenin, F., Martinerie,
746 P., Ritz, C., Capron, E., and Lipenkov, V.: An optimized multi-proxy, multi-site Antarctic ice and
747 gas orbital chronology (AICC2012): 120-800 ka, *Clim. Past.*, 9, 1715-1731, 2013.
- 748 Bergin, M. H., Meyerson, E. A., Dibb, J. E., and Mayewski, P. A.: Relationship between
749 continuous aerosol measurements and firn core chemistry over a 10-year period at the South Pole,
750 *Geophys. Res. Lett.*, 25, 1189-1192, 1998.
- 751 Bodhaine, B. A., Deluisi, J. J., Harris, J. M., Houmère, P., and Bauman, S.: Aerosol
752 measurements at the South Pole, *Tellus B: Chemical and Physical Meteorology*, 38, 223-235,
753 1986.
- 754 Breton, D. J., Koffman, B. G., Kurbatov, A. V., Kreutz, K. J., and Hamilton, G. S.: Quantifying
755 signal dispersion in a hybrid ice core melting system, *Environ. Sci. Technol.*, 46, 11922-11928,
756 2012.
- 757 Budner, D., and Cole-Dai, J.: The number and magnitude of large explosive volcanic eruptions
758 between 904 and 1865 AD: Quantitative evidence from a new South Pole ice core, *Volcanism*
759 *and the Earth's Atmosphere*, 165-176, 2003.
- 760 Buizert, C., Cuffey, K. M., Severinghaus, J. P., Baggenstos, D., Fudge, T. J., Steig, E. J., Markle,
761 B. R., Winstrup, M., Rhodes, R. H., and Brook, E. J.: The WAIS Divide deep ice core WD2014
762 chronology—Part 1: Methane synchronization (68–31 ka BP) and the gas age–ice age difference,
763 *Clim. Past.*, 11, 153-173, 2015.
- 764 Buizert, C., Gkinis, V., Severinghaus, J. P., He, F., Lecavalier, B. S., Kindler, P., Leuenberger,
765 M., Carlson, A. E., Vinther, B., and Masson-Delmotte, V.: Greenland temperature response to
766 climate forcing during the last deglaciation, *Science*, 345, 1177-1180, 2014.



- 767 Buizert, C., Sigl, M., Severi, M., Markle, B. R., Wettstein, J. J., McConnell, J. R., Pedro, J. B.,
768 Sodemann, H., Goto-Azuma, K., and Kawamura, K.: Abrupt ice-age shifts in southern westerly
769 winds and Antarctic climate forced from the north, *Nature*, 563, 681, 2018.
- 770 Casey, K. A., Fudge, T. J., Neumann, T. A., Steig, E. J., Cavitte, M. G. P., and Blankenship, D.
771 D.: The 1500 m South Pole ice core: recovering a 40 ka environmental record, *Ann. Glaciol.*, 55,
772 137-146, 2014.
- 773 Casey, K. A., Kaspari, S. D., Skiles, S. M., Kreutz, K., and Handley, M. J.: The spectral and
774 chemical measurement of pollutants on snow near South Pole, Antarctica, *Journal of Geophysical*
775 *Research: Atmospheres*, 122, 6592-6610, 2017.
- 776 Cole-Dai, J., and Mosley-Thompson, E.: The Pinatubo eruption in South Pole snow and its
777 potential value to ice-core paleovolcanic records, *Ann. Glaciol.*, 29, 99-105, 1999.
- 778 Cole-Dai, J., Ferris, D., Lanciki, A., Savarino, J., Baroni, M., and Thiemens, M. H.: Cold decade
779 (AD 1810–1819) caused by Tambora (1815) and another (1809) stratospheric volcanic eruption,
780 *Geophys. Res. Lett.*, 36, 2009.
- 781 Cole-Dai, J., Mosley-Thompson, E., Wight, S. P., and Thompson, L. G.: A 4100-year record of
782 explosive volcanism from an East Antarctica ice core, *Journal of Geophysical Research:*
783 *Atmospheres*, 105, 24431-24441, 2000.
- 784 Curran, M. A. J., Van Ommen, T. D., and Morgan, V.: Seasonal characteristics of the major ions
785 in the high-accumulation Dome Summit South ice core, Law Dome, Antarctica, *Ann. Glaciol.*,
786 27, 385-390, 1998.
- 787 Dansgaard, W., and Johnsen, S. J.: A flow model and a time scale for the ice core from Camp
788 Century, Greenland, *J. Glaciol.*, 8, 215-223, 1969.
- 789 Davis, D., Chen, G., Buhr, M., Crawford, J., Lenschow, D., Lefer, B., Shetter, R., Eisele, F.,
790 Mauldin, L., and Hogan, A.: South Pole NO_x chemistry: an assessment of factors controlling
791 variability and absolute levels, *Atmos. Environ.*, 38, 5375-5388, 2004.
- 792 Delmas, R. J., Kirchner, S., Palais, J. M., and Petit, J. R.: 1000 years of explosive volcanism
793 recorded at the South Pole, *Tellus B*, 44, 335-350, 1992.
- 794 Ekaykin, A. A., Lipenkov, V. Y., Kuzmina, I. N., Petit, J. R., Masson-Delmotte, V., and Johnsen,
795 S. J.: The changes in isotope composition and accumulation of snow at Vostok station, East
796 Antarctica, over the past 200 years, *Ann. Glaciol.*, 39, 569-575, 2004.
- 797 Erbland, J., Vicars, W. C., Savarino, J., Morin, S., Frey, M. M., Frosini, D., Vince, E., and
798 Martins, J. M. F.: Air–snow transfer of nitrate on the East Antarctic Plateau—Part 1: Isotopic
799 evidence for a photolytically driven dynamic equilibrium in summer, *Atmos. Chem. Phys.*, 13,
800 6403-6419, 2013.
- 801 Fegyveresi, J. M., Fudge, T. J., Winski, D. A., Ferris, D. G.: Visual Observations and
802 Stratigraphy of the South Pole Ice Core, ERDC/CRREL Report No. TR-19. ERDC-CRREL
803 Hanover, NH, United States, 2017.
- 804 Ferris, D. G., Cole-Dai, J., Reyes, A. R., and Budner, D. M.: South Pole ice core record of
805 explosive volcanic eruptions in the first and second millennia AD and evidence of a large



- 806 eruption in the tropics around 535 AD, *J. Geophys. Res.-Atmos.*, 116, 10.1029/2011jd015916,
807 2011.
- 808 Fudge, T. J., Taylor, K. C., Waddington, E. D., Fitzpatrick, J. J., and Conway, H.: Electrical
809 stratigraphy of the WAIS Divide ice core: Identification of centimeter-scale irregular layering,
810 *Journal of Geophysical Research: Earth Surface*, 121, 1218-1229, 2016a.
- 811 Fudge, T. J., Markle, B. R., Cuffey, K. M., Buizert, C., Taylor, K. C., Steig, E. J., Waddington, E.
812 D., Conway, H., and Koutnik, M.: Variable relationship between accumulation and temperature
813 in West Antarctica for the past 31,000 years, *Geophys. Res. Lett.*, 43, 3795-3803, 2016b.
- 814 Fudge, T. J., Waddington, E. D., Conway, H., Lundin, J. M. D., and Taylor, K.: Interpolation
815 methods for Antarctic ice-core timescales: application to Byrd, Siple Dome and Law Dome ice
816 cores, *Clim. Past.*, 10, 1195-1209, 2014.
- 817 Fujita, S., Parrenin, F., Severi, M., Motoyama, H., and Wolff, E. W.: Volcanic synchronization of
818 Dome Fuji and Dome C Antarctic deep ice cores over the past 216 kyr, *Clim. Past.*, 11, 1395-
819 1416, 2015.
- 820 Goujon, C., Barnola, J. M., and Ritz, C.: Modeling the densification of polar firn including heat
821 diffusion: Application to close-off characteristics and gas isotopic fractionation for Antarctica and
822 Greenland sites, *Journal of Geophysical Research: Atmospheres*, 108, 2003.
- 823 Gow, A. J.: On the accumulation and seasonal stratification of snow at the South Pole, *J. Glaciol.*,
824 5, 467-477, 1965.
- 825 Grannas, A. M., Jones, A. E., Dibb, J., Ammann, M., Anastasio, C., Beine, H. J., Bergin, M.,
826 Bottenheim, J., Boxe, C. S., and Carver, G.: An overview of snow photochemistry: evidence,
827 mechanisms and impacts, *Atmos. Chem. Phys.*, 7, 4329-4373, 2007.
- 828 Hamilton, G. S.: Topographic control of regional accumulation rate variability at South Pole and
829 implications for ice-core interpretation, *Ann. Glaciol.*, 39, 214-218, 2004.
- 830 Herron, M. M., and Langway, C. C.: Firn densification: an empirical model, *J. Glaciol.*, 25, 373-
831 385, 1980.
- 832 Hogan, A.: A synthesis of warm air advection to the South Polar Plateau, *Journal of Geophysical
833 Research: Atmospheres*, 102, 14009-14020, 1997.
- 834 Hogan, A. W., and Gow, A. J.: Occurrence frequency of thickness of annual snow accumulation
835 layers at South Pole, *Journal of Geophysical Research: Atmospheres*, 102, 14021-14027, 1997.
- 836 Johnson, J. A., Shturmakov, A. J., Kuhl, T. W., Mortensen, N. B., and Gibson, C. J.: Next
837 generation of an intermediate depth drill, *Ann. Glaciol.*, 55, 27-33, 2014.
- 838 Jones, T. R., White, J. W. C., Steig, E. J., Vaughn, B. H., Morris, V., Gkinis, V., Markle, B. R.,
839 and Schoenemann, S. W.: Improved methodologies for continuous-flow analysis of stable water
840 isotopes in ice cores, *Atmospheric Measurement Techniques*, 10, 2017.
- 841 Kaspari, S., Hooke, R. L., Mayewski, P. A., Kang, S., Hou, S., and Qin, D.: Snow accumulation
842 rate on Qomolangma (Mount Everest), Himalaya: synchronicity with sites across the Tibetan
843 Plateau on 50–100 year timescales, *J. Glaciol.*, 54, 343-352, 2008.



- 844 Koffman, B. G., Kreutz, K. J., Breton, D. J., Kane, E. J., Winski, D. A., Birkel, S. D., Kurbatov,
845 A. V., and Handley, M. J.: Centennial-scale variability of the Southern Hemisphere westerly wind
846 belt in the eastern Pacific over the past two millennia, *Clim. Past.*, 10, 1125-1144, 2014.
- 847 Korotkikh, E. V., Mayewski, P. A., Dixon, D., Kurbatov, A. V., and Handley, M. J.: Recent
848 increase in Ba concentrations as recorded in a South Pole ice core, *Atmos. Environ.*, 89, 683-687,
849 2014.
- 850 Koutnik, M. R., Fudge, T. J., Conway, H., Waddington, E. D., Neumann, T. A., Cuffey, K. M.,
851 Buizert, C., and Taylor, K. C.: Holocene accumulation and ice flow near the West Antarctic Ice
852 Sheet Divide ice core site, *Journal of Geophysical Research: Earth Surface*, 121, 907-924, 2016.
- 853 Kreutz, K. J., Mayewski, P. A., Meeker, L. D., Twickler, M. S., Whitlow, S. I., and Pittalwala, II:
854 Bipolar changes in atmospheric circulation during the Little Ice Age, *Science*, 277, 1294-1296,
855 10.1126/science.277.5330.1294, 1997.
- 856 Kuivinen, K. C., Koci, B. R., Holdsworth, G. W., and Gow, A. J.: South Pole ice core drilling,
857 1981–1982, *Antarct. JUS*, 17, 89-91, 1982.
- 858 Lazzara, M. A., Keller, L. M., Markle, T., and Gallagher, J.: Fifty-year Amundsen–Scott South
859 Pole station surface climatology, *Atmos. Res.*, 118, 240-259, 2012.
- 860 Legrand, M. R., and Delmas, R. J.: The ionic balance of Antarctic snow: a 10-year detailed
861 record, *Atmospheric Environment* (1967), 18, 1867-1874, 1984.
- 862 Lilien, D., Fudge, T. J., Koutnik, M., Conway, H., Osterberg, E., Ferris, D., Waddington, E.,
863 Stevens, C. M., and Welten, K. C.: Holocene ice-flow speedup in the vicinity of South Pole,
864 submitted, 2018.
- 865 Lundin, J. M. D., Stevens, C. M., Arthern, R., Buizert, C., Orsi, A., Ligtenberg, S. R. M.,
866 Simonsen, S. B., Cummings, E., Essery, R., and Leahy, W.: Firm Model Intercomparison
867 Experiment (FirmMICE), *J. Glaciol.*, 63, 401-422, 2017.
- 868 Meyerson, E. A., Mayewski, P. A., Kreutz, K. J., Meeker, L. D., Whitlow, S. I., and Twickler, M.
869 S.: The polar expression of ENSO and sea-ice variability as recorded in a South Pole ice core, in:
870 *Annals of Glaciology*, Vol 35, edited by: Wolff, E. W., *Annals of Glaciology*, 430-436, 2002.
- 871 Monaghan, A. J., Bromwich, D. H., Fogt, R. L., Wang, S.-H., Mayewski, P. A., Dixon, D. A.,
872 Ekaykin, A., Frezzotti, M., Goodwin, I., and Isaksson, E.: Insignificant change in Antarctic
873 snowfall since the International Geophysical Year, *Science*, 313, 827-831, 2006.
- 874 Mosley-Thompson, E., Kruss, P. D., Thompson, L. G., Pourchet, M., and Grootes, P.: Snow
875 stratigraphic record at South Pole: potential for paleoclimatic reconstruction, *Ann. Glaciol.*, 7, 26-
876 33, 1985.
- 877 Mosley-Thompson, E., Paskievitch, J. F., Gow, A. J., and Thompson, L. G.: Late 20th Century
878 increase in South Pole snow accumulation, *J. Geophys. Res.-Atmos.*, 104, 3877-3886,
879 10.1029/1998jd200092, 1999.
- 880 Mosley-Thompson, E., and Thompson, L. G.: Nine Centuries of Microparticle Deposition at the
881 South Pole I, *Quat. Res.*, 17, 1-13, 1982.



- 882 Mosley-Thompson, E., Thompson, L. G., Paskievitch, J. F., Pourchet, M., Gow, A. J., Davis, M.
883 E., and Kleinman, J.: Recent increase in South Pole snow accumulation, *Ann. Glaciol.*, 21, 131-
884 138, 1995.
- 885 Munger, J. W., Jacob, D. J., Fan, S. M., Colman, A. S., and Dibb, J. E.: Concentrations and
886 snow-atmosphere fluxes of reactive nitrogen at Summit, Greenland, *Journal of Geophysical*
887 *Research: Atmospheres*, 104, 13721-13734, 1999.
- 888 Osterberg, E. C., Handley, M. J., Sneed, S. B., Mayewski, P. A., and Kreutz, K. J.: Continuous
889 ice core melter system with discrete sampling for major ion, trace element, and stable isotope
890 analyses, *Environ. Sci. Technol.*, 40, 3355-3361, 10.1021/es052536w, 2006.
- 891 Osterberg, E. C., Winski, D. A., Kreutz, K. J., Wake, C. P., Ferris, D. G., Campbell, S., Introne,
892 D., Handley, M., and Birkel, S.: 1200-Year Composite Ice Core Record of Aleutian Low
893 Intensification, *Geophys. Res. Lett.*, 2017.
- 894 Palais, J. M., Kirchner, S., and Delmas, R. J.: Identification of some global volcanic horizons by
895 major element analysis of fine ash in Antarctic ice, *Ann. Glaciol.*, 14, 216-220, 1990.
- 896 Parrenin, F., Remy, F., Ritz, C., Siegert, M. J., and Jouzel, J.: New modeling of the Vostok ice
897 flow line and implication for the glaciological chronology of the Vostok ice core, *Journal of*
898 *Geophysical Research: Atmospheres*, 109, 2004.
- 899 Parungo, F., Bodhaine, B., and Bortniak, J.: Seasonal variation in Antarctic aerosol, *Journal of*
900 *aerosol science*, 12, 491-504, 1981.
- 901 Petit, J. R., Jouzel, J., Pourchet, M., and Merlivat, L.: A detailed study of snow accumulation and
902 stable isotope content in Dome C (Antarctica), *Journal of Geophysical Research: Oceans*, 87,
903 4301-4308, 1982.
- 904 Petrenko, V. V., Severinghaus, J. P., Brook, E. J., Reeh, N., and Schaefer, H.: Gas records from
905 the West Greenland ice margin covering the Last Glacial Termination: a horizontal ice core,
906 *Quat. Sci. Rev.*, 25, 865-875, 2006.
- 907 Röthlisberger, R., Hutterli, M. A., Sommer, S., Wolff, E. W., and Mulvaney, R.: Factors
908 controlling nitrate in ice cores: Evidence from the Dome C deep ice core, *Journal of Geophysical*
909 *Research: Atmospheres*, 105, 20565-20572, 2000.
- 910 Röthlisberger, R., Hutterli, M. A., Wolff, E. W., Mulvaney, R., Fischer, H., Bigler, M., Goto-
911 Azuma, K., Hansson, M. E., Ruth, U., and Siggaard-Andersen, M.-L.: Nitrate in Greenland and
912 Antarctic ice cores: a detailed description of post-depositional processes, *Ann. Glaciol.*, 35, 209-
913 216, 2002.
- 914 Ruth, U., Barnola, J. M., Beer, J., Bigler, M., Blunier, T., Castellano, E., Fischer, H., Fundel, F.,
915 Huybrechts, P., and Kaufmann, P.: "EDML1": a chronology for the EPICA deep ice core from
916 Dronning Maud Land, Antarctica, over the last 150 000 years, *Climate of the Past Discussions*, 3,
917 549-574, 2007.
- 918 Severi, M., Becagli, S., Castellano, E., Morganti, A., Traversi, R., Udisti, R., Ruth, U., Fischer,
919 H., Huybrechts, P., and Wolff, E.: Synchronisation of the EDML and EDC ice cores for the last
920 52 kyr by volcanic signature matching, *Climate of the Past Discussions*, 3, 409-433, 2007.



- 921 Severi, M., Udisti, R., Becagli, S., Stenni, B., and Traversi, R.: Volcanic synchronisation of the
922 EPICA-DC and TALDICE ice cores for the last 42 kyr BP, *Clim. Past.*, 8, 509-517, 2012.
- 923 Severinghaus, J. P., Sowers, T., Brook, E. J., Alley, R. B., and Bender, M. L.: Timing of abrupt
924 climate change at the end of the Younger Dryas interval from thermally fractionated gases in
925 polar ice, *Nature*, 391, 141, 1998.
- 926 Sigl, M., Fudge, T. J., Winstrup, M., Cole-Dai, J., Ferris, D., McConnell, J. R., Taylor, K. C.,
927 Welten, K. C., Woodruff, T. E., and Adolphi, F.: The WAIS Divide deep ice core WD2014
928 chronology–Part 2: Annual-layer counting (0–31 ka BP), *Clim. Past.*, 12, 769-786, 2016.
- 929 Sigl, M., McConnell, J. R., Layman, L., Maselli, O., McGwire, K., Pasteris, D., Dahl-Jensen, D.,
930 Steffensen, J. P., Vinther, B., Edwards, R., Mulvaney, R., and Kipfstuhl, S.: A new bipolar ice
931 core record of volcanism from WAIS Divide and NEM and implications for climate forcing of
932 the last 2000 years, *J. Geophys. Res.-Atmos.*, 118, 1151-1169, 10.1029/2012jd018603, 2013.
- 933 Souney, J. M., Twickler, M. S., Hargreaves, G. M., Bencivengo, B. M., Kippenhan, M. J.,
934 Johnson, J. A., Cravens, E. D., Neff, P. D., Nunn, R. M., and Orsi, A. J.: Core handling and
935 processing for the WAIS Divide ice-core project, *Ann. Glaciol.*, 55, 15-26, 2014.
- 936 Sowers, T., Bender, M., Raynaud, D., and Korotkevich, Y. S.: $\delta^{15}\text{N}$ of N_2 in air trapped in polar
937 ice: A tracer of gas transport in the firm and a possible constraint on ice age-gas age differences,
938 *Journal of Geophysical Research: Atmospheres*, 97, 15683-15697, 1992.
- 939 Thompson, L. G., Davis, M. E., Mosley-Thompson, E., Sowers, T. A., Henderson, K. A.,
940 Zagorodnov, V. S., Lin, P. N., Mikhalevko, V. N., Campen, R. K., and Bolzan, J. F.: A 25,000-
941 year tropical climate history from Bolivian ice cores, *Science*, 282, 1858-1864, 1998.
- 942 Torrence, C., and Compo, G. P.: A practical guide to wavelet analysis, *Bull. Amer. Meteorol.*
943 *Soc.*, 79, 61-78, 1998.
- 944 Udisti, R., Dayan, U., Becagli, S., Busetto, M., Frosini, D., Legrand, M., Lucarelli, F., Preunkert,
945 S., Severi, M., and Traversi, R.: Sea spray aerosol in central Antarctica. Present atmospheric
946 behaviour and implications for paleoclimatic reconstructions, *Atmos. Environ.*, 52, 109-120,
947 2012.
- 948 van der Veen, C. J., Mosley-Thompson, E., Gow, A. J., and Mark, B. G.: Accumulation At South
949 Pole: Comparison of two 900-year records, *J. Geophys. Res.-Atmos.*, 104, 31067-31076,
950 10.1029/1999jd900501, 1999.
- 951 Veres, D., Bazin, L., Landais, A., Toyé Mahamadou Kele, H., Lemieux-Dudon, B., Parrenin, F.,
952 Martinerie, P., Blayo, E., Blunier, T., and Capron, E.: The Antarctic ice core chronology
953 (AICC2012): an optimized multi-parameter and multi-site dating approach for the last 120
954 thousand years, *Clim. Past.*, 9, 1733-1748, 2013.
- 955 Waddington, E. D., Neumann, T. A., Koutnik, M. R., Marshall, H.-P., and Morse, D. L.:
956 Inference of accumulation-rate patterns from deep layers in glaciers and ice sheets, *J. Glaciol.*, 53,
957 694-712, 2007.
- 958 Wagenbach, D., Ducroz, F., Mulvaney, R., Keck, L., Minikin, A., Legrand, M., Hall, J. S., and
959 Wolff, E. W.: Sea-salt aerosol in coastal Antarctic regions, *Journal of Geophysical Research:*
960 *Atmospheres*, 103, 10961-10974, 1998.



- 961 Whitlow, S., Mayewski, P. A., and Dibb, J. E.: A comparison of major chemical species seasonal
962 concentration and accumulation at the South Pole and Summit, Greenland, Atmospheric
963 Environment. Part A. General Topics, 26, 2045-2054, 1992.
- 964 Winski, D., Osterberg, E. F., D. Kreutz, K., Wake, C. C., S. Hawley, R., Roy, S., and Birkel, S. I.,
965 D. Handley, M.: Industrial-age doubling of snow accumulation in the Alaska Range linked to
966 tropical ocean warming, Nature Scientific Reports, 2017.
- 967 Winstrup, M., Svensson, A. M., Rasmussen, S. O., Winther, O., Steig, E. J., and Axelrod, A. E.:
968 An automated approach for annual layer counting in ice cores, Clim. Past, 8, 1881-1895,
969 10.5194/cp-8-1881-2012, 2012.